Eur Biophys J (2009) 38:613–624
DOI 10.1007/s00249-009-0415-3

ORIGINAL PAPER

Perturbation of DPPC/POPG bilayers by the N-terminal helix of lung surfactant protein SP-B: a ^{2}H NMR study

Bretta Russell-Schulz · Valerie Booth · Michael R. Morrow

Received: 23 October 2008 / Revised: 30 January 2009 / Accepted: 2 February 2009 / Published online: 18 February 2009

Abstract SP-$B_{8–25}$ is a synthetic peptide comprising the N-terminal helix of the essential lung surfactant protein SP-B. Rat lung oxygenation studies have shown that SP-$B_{8–25}$ retains some of the function of full-length SP-B. We have used deuterium nuclear magnetic resonance (^{2}H-NMR) to examine the influence of SP-$B_{8–25}$ on the mixing properties of saturated PC and unsaturated PG lipids in model mixed lipid bilayers containing dipalmitoylphosphatidylcholine (DPPC) and palmitoyl-oleoyl-phosphatidylglycerol (POPG), in a molar ratio of 7:3. In the absence of the peptide, ^{2}H-NMR spectra of DPPC/POPG mixtures, with one or the other lipid component deuterated, indicate coexistence of large liquid crystal and gel domains over a range of about 10°C through the liquid crystal to gel transition of the bilayer. Addition of SP-$B_{8–25}$ has little effect on the width of the transition but the spectra through the transition range cannot be resolved into distinct liquid crystal and gel spectral components suggesting that the peptide interferes with the tendency of the DPPC and POPG lipid components in this mixture to phase separate near the bilayer transition temperature. Quadrupole echo decay observations suggest that the peptide may also reduce differences in the correlation times for local reorientation of the two lipids. These observations suggest that SP-$B_{8–25}$ promotes a more thorough mixing of saturated PC and unsaturated PG components and may be relevant to understanding the behaviour of lung surfactant material under conditions of lateral compression which might be expected to enhance the propensity for saturated and unsaturated surfactant lipid components to segregate.

Keywords Lung surfactant protein · SP-B N-terminal peptide · ^{2}H-NMR · Phase separation · Dipalmitoylphosphatidylcholine (DPPC) · Palmitoyl-oleoyl-phosphatidylglycerol (POPG)

B. Russell-Schulz · V. Booth · M. R. Morrow (✉)
Department of Physics and Physical Oceanography,
Memorial University of Newfoundland,
St. John's, NF A1B 3X7, Canada
e-mail: mmorrow@mun.ca

B. Russell-Schulz · V. Booth
Department of Biochemistry,
Memorial University of Newfoundland,
St. John's, NF A1B 3X7, Canada

Introduction

Respiration is facilitated by a surfactant layer that reduces surface tension at the air–water interface in alveoli (Pattle 1955; Clements 1957). The surface active layer is composed of a lipid–protein mixture initially secreted in the form of lamellar bodies by alveolar type II cells (Perez-Gil and Keough 1998). Approximately 90% of the dry surfactant material mass is lipid and ~85–90% of the lipid is phospholipid (Yu et al. 1983; Goerke 1998; Veldhuizen et al. 1998). Approximately 80% of the phospholipid is phosphatidylcholine (PC) and ~10% is phosphatidylglycerol (PG) (Veldhuizen et al. 1998; Postle et al. 2001). Up to half of the PC and most of the non-PC phospholipid is unsaturated (Zuo et al. 2008a). While lateral compression of monolayers enriched in dipalmitoylphosphatidylcholine (DPPC) can reduce surface tension at the air–water interface, in vivo effectiveness also depends on the presence of additional components, including unsaturated lipids, anionic lipids, surfactant proteins, and Ca^{2+}, that influence the rate of surfactant material adsorption to the air–water interface (Keough 1998; Zuo et al. 2008a).

Four proteins account for ~10% of surfactant dry weight (Yu et al. 1983; Goerke 1998). Of these, the two hydrophobic proteins, SP-B and SP-C, are thought to facilitate adsorption and spreading of surfactant lipid material from lamellar reservoirs to the surface active layer and to facilitate association of multilayer structures with the surface active layer during expiration (Perez-Gil and Keough 1998; Goerke 1998; Zuo et al. 2008a). SP-B is the lung surfactant protein with the strongest capacity to promote lipid adsorption and surface tension reduction at the air–water interface (Revak et al. 1988) and is the only one essential for life (Nogee et al. 1994; Clark et al. 1995).

SP-B monomers (molecular mass 8.7 kDa) have 79 amino acids including six cysteines that form three intramolecular disulphide bonds (Johansson et al. 1991; Hawgood et al. 1998). Another cysteine participates in an intermolecular bridge so that SP-B forms a 17.4 kDa dimer in its native state (Beck et al. 2000). SP-B monomers contain four amphipatic, α-helical regions and an overall positive charge (Vandenbussche et al. 1992; Andersson et al. 1995). ^{2}H-NMR has been used to study the interaction of SP-B with DPPC alone (Morrow et al. 1993, 2004) and with one or both components in DPPC/dipalmitoylphosphatidylglycerol (DPPG) mixtures (Dico et al. 1997; Morrow et al. 2007). Large SP-B concentrations (~17% w/w) qualitatively altered lipid chain packing in 1,2-perdeuterodipalmitoyl-*sn*-glycero-3-phosphocholine (DPPC-d_{62}) bilayers (Morrow et al. 2004). At 13% (w/w) in mixtures of DPPC/DPPG (7:3), SP-B was found to lower the chain orientational order of both lipid components, slightly, both above and below the main transition (Morrow et al. 2007). SP-B did not significantly change the transition width in DPPC-d_{62}/DPPG (7:3) but slightly narrowed the transition in DPPC/DPPG-d_{62} (7:3).

Various peptides based on segments of SP-B have been studied. High resolution NMR structural studies have been done on an N-terminal-based SP-B peptide (SP-$B_{11–25}$) in methanol (Kurutz and Lee 2002), a C-terminal-based peptide (SP-$B_{63–78}$) both in organic solvent and in sodium dodecyl sulphate (SDS) micelles (Booth et al. 2004), and a peptide comprising SP-B residues 8–25 and 63–78 (termed mini-B), also incorporated into SDS micelles (Sarker et al. 2007). All retained substantial regions of amphipathic, α-helical conformation.

In this study, we used ^{2}H-NMR to study the interaction of an SP-B N-terminal peptide fragment (SP-$B_{8–25}$) with both lipid components of bilayers containing DPPC and 1-palmitoyl-2-oleoyl-*sn*-glycero-3-phosphoglycerol (POPG) in a molar ratio of 7:3. SP-$B_{8–25}$ includes the first amphipathic α-helical portion of SP-B and has a net charge of +4. Surfactant preparations containing N-terminal helical fragments of SP-B enhance oxygenation and lung compliance in surfactant-deficient animal models (Revak et al. 1991; Walther et al. 2002) and biophysical properties such as surface tension reduction and dynamic respreading (Veldhuizen et al. 2000; Ryan et al. 2005; Serrano et al. 2006). The N-terminal fragment chosen for this study includes a tryptophan residue (position 9) that appears to be key in the function of full-length SP-B, since its oxidative modification has severe effects on the activity of surfactant (Serrano et al. 2006; Manzanares et al. 2007). Knowledge of how specific SP-B segments interact with lipid materials contributes to understanding of the relationship between structure of the complete SP-B molecule and its functional role in surfactant and also supports the development of improved artificial surfactants with suitable SP-B fragments in place of animal-derived full-length SP-B.

The primary focus in this work is on how SP-$B_{8–25}$ affects lipid mixing properties and domain growth in a model surfactant mixture containing saturated PC and monounsaturated PG lipids. The selected lipid composition facilitates comparison with other studies in which a 7:3 PC/PG ratio has been used to model lipid components of surfactant material. This lipid composition is popular for biophysical studies of lung surfactant components (e.g. Pastrana-Rios et al. 1994; Zasadzinski et al. 2001; Antharam et al. 2008) because it approximates the physiological ratio of saturated and unsaturated chains and provides significant anionic lipid content. An important difference between this study and an earlier one involving DPPC/DPPG mixtures (Morrow et al. 2007) is that the lipid composition in the current study more closely approximates the ratio of saturated to unsaturated chains in lung surfactant. This is significant because domain formation is potentially relevant to lung surfactant function (Zuo et al. 2008a) and the mixing properties of saturated and unsaturated lipid components may affect the lateral distribution of components in functional surfactant. Using ^{2}H-NMR to examine phase separation in nominally identical mixtures, with one or the other lipid deuterated, provides an indication of the extent to which interaction with SP-$B_{8–25}$ influences the mixing properties of lipid components in this model surfactant mixture.

Materials and methods

Lipids

Dipalmitoylphosphatidylcholine, POPG, and their chain-deuterated versions DPPC-d_{62} and POPG-d_{31} were all purchased from Avanti Polar Lipids Inc. (Alabaster, AL) and used without further purification.

Polypeptide

Synthetic polypeptide based on the N-terminal segment of surfactant protein B (SP-$B_{8–25}$) was purchased from the University of Calgary Peptide Services (Calgary, Canada) where it was produced by solid phase peptide synthesis and purified to >90% purity by high-pressure liquid chromatography. The peptide stock was stored in dry form at −20°C.

Bilayer sample preparation

Bilayer preparation was modelled on an approach used earlier (Morrow et al. 2007). The lipid mixtures, either DPPC-d_{62} plus POPG (7:3) or DPPC plus POPG-d_{31} (7:3), were first dissolved and mixed in chloroform/methanol 1:1 (v/v). For each sample, total lipid mass was about 25 mg. Lipid concentration in each sample was determined using phosphorus analysis (Bartlett 1959; Keough and Kariel 1987). For samples containing peptide, dry SP-$B_{8–25}$ was weighed out and added so that peptide was 3.5% of the total mass. This is equivalent to 1 peptide molecule per 76 lipid molecules, a molar peptide: lipid ratio similar to that used in a previous study with full-length SP-B (Morrow et al. 2007). Solvent was removed by rotary evaporation at ~50°C followed by at least 8 h of further drying under vacuum. Dry samples were hydrated using 10 mL of buffer (10 mM TRIS/145 mM NaCl/1 mM EDTA in deuterium-depleted water, pH 7.4) at 46°C with vortexing every 10 min for 1 h. A 2-ml aliquot was removed for analysis by differential scanning calorimetry. The remaining 8 ml volume of each sample was then centrifuged at 50,000*g* and 4°C for 30 min. The supernatant was removed after which the pellet was re-suspended in 1 ml of supernatant. Calcium chloride in solution was added to achieve an overall Ca^{2+} concentration of 5 mM in a 4 ml volume of sample suspension. The sample was centrifuged again at 5,000*g* for 15 min to remove excess buffer. The resulting suspension was transferred to a 400 µl NMR tube. To test for reproducibility, two samples of each peptide-containing sample were prepared independently and subjected to the same series of experiments.

^{2}H-NMR

Wideline ^{2}H-NMR experiments were performed using a locally constructed spectrometer utilising a 9.4 T superconducting solenoid (Magnex Scientific, Concord, CA). Spectra were acquired using a quadrupole echo pulse sequence (Davis et al. 1976) comprising a pair of $\pi/2$ pulses (3.7–4 µs) separated by a 35 µs delay. Free-induction decays were acquired with a 1 µs dwell time and oversampling to give effective dwell times of 4 and 2 µs for liquid crystalline and gel phase samples, respectively (Prosser et al. 1991). The number of transients averaged was typically 4,000 for samples containing DPPC-d_{62} and 4,000–16,000 for samples containing POPG-d_{31}. Spectra used for first spectral moments were symmetrised by zeroing the imaginary channel before Fourier transformation.

The sample tube and probe coil were enclosed in a copper oven and maintained to within ± 0.1° of selected temperatures using a digital temperature controller (model 325, LakeShore Cryotronics, Westerville, OH). Data collection started at 44°C and decreased in steps of 2°C down to 10°C with a final step to 5°C. Samples were allowed to equilibrate for at least 20 min after each cooling step before data collection.

Differential scanning calorimetry (DSC)

Differential scanning calorimetry scans were performed using a Microcal (Northhampton, MA) MC-2 instrument. Each of the sample suspensions scanned contained 3 mg of lipid. Following equilibration at ~12°C, each sample was scanned at 30°C/h. Using Origin 6.1 (OriginLab Corp., Northhampton, MA), segments of baseline spanning a few degrees above and below the transition on each scan were selected and fit to a quadratic. The resulting baseline function was subtracted from each scan to give ΔC_p versus temperature. Each sample was scanned at least twice.

Results

Figure 1 shows spectra at selected temperatures for dispersions of DPPC-d_{62}/POPG (7:3) and DPPC/POPG-d_{31} (7:3), both without peptide, and for both lipid mixtures with 3.5 % (w/w) SP-$B_{8–25}$ incorporated. At high temperature, spectra for all samples are superpositions of Pake doublets characteristic of fast, axially symmetric reorientation of the deuterium-labelled saturated chain in liquid crystalline phase multilamellar vesicles. The distribution of doublet splitting reflects variation of orientational order with position along the chain. The liquid crystalline spectra for DPPC-d_{62}/POPG (7:3) (Fig. 1a) are characterised by limited resolution. Similar resolution was observed from a second preparation of DPPC-d_{62}/POPG and may reflect perturbation of DPPC-d_{62} dynamics by POPG. At low temperatures, the spectra are characteristic of more ordered chains undergoing reorientation that is not axially symmetric on the characteristic time scale (~10^{-5} s) of the ^{2}H-NMR experiment. These spectra do not provide a basis for distinguishing between the P_β' and L_β' phases and we will simply identify them as characteristic of the gel phase. Intensity in the gel phase spectra extends to about twice the

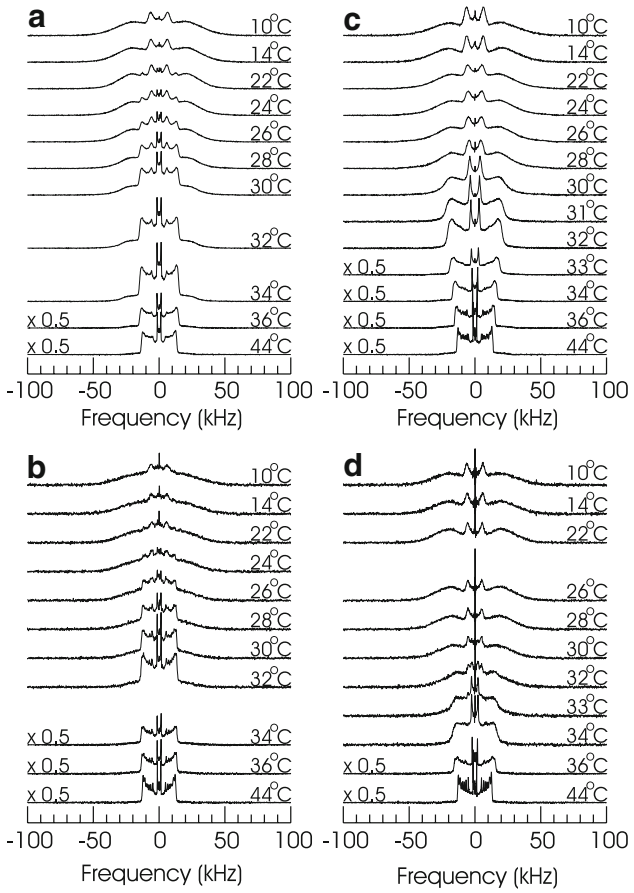

Fig. 1 ^{2}H-NMR spectra at selected temperatures for **a** DPPC-d_{62}/POPG (7:3), **b** DPPC/POPG-d_{31} (7:3), **c** DPPC-d_{62}/POPG (7:3) + 3.5% N-terminal SP-B peptide and **d** DPPC/POPG-d_{31} (7:3) + 3.5% N-terminal SP-B peptide. All samples were hydrated in TRIS buffer containing 5 mM Ca^{2+} at pH 7.4

maximum splitting for the liquid crystalline phase spectra. The prominent feature spanning 15–20 kHz, in the low-temperature spectra, arises from deuterated chain methyl groups which continue to reorient rapidly in the gel phase.

Spectra for the samples with and without SP-$B_{8–25}$ incorporated are distinguished by their behaviour in the temperature range spanning the liquid crystal to gel transition. For DPPC-d_{62}/POPG (7:3) (Fig. 1a), gel phase spectral characteristics begin to emerge as the sample is cooled through 36°C. From this temperature down to ~18°C, the DPPC-d_{62}/POPG (7:3) spectra are superpositions of liquid crystal and gel spectral components implying a broad range of two phase coexistence in the DPPC/POPG temperature-composition phase diagram. Observation of distinct liquid crystal and gel spectral components implies that coexisting domains are large enough that spectral averaging due to diffusion across domain boundaries can be neglected over the characteristic time scale of the ^{2}H-NMR experiment. At 16°C, liquid crystalline features are effectively absent. The DPPC/POPG-d_{31} (7:3) spectra (Fig. 1b) indicate coexistence of liquid crystal and gel phase domains over a similar range of temperatures. Taking into account the effect, on transition temperatures, of deuterating one or the other lipid component in each mixture, the upper limit of two phase coexistence seen for this mixture is consistent with the liquidus line in the DPPC/POPG phase diagram obtained earlier using DSC and ^{13}C-NMR (Wiedmann et al. 1993). The liquid crystalline spectral components seen here persist to slightly lower temperature than might be expected from the earlier work.

Acyl chain perdeuteration lowers the transition for DPPC-d_{62} bilayers by ~4°C relative to the transition for unlabelled DPPC bilayers (Davis 1979). The downward shift in the transition for DPPC-d_{62}/POPG (7:3), relative to the corresponding transition for the same mixture with no deuterium-labelled lipid, is expected to be slightly larger than the shift for DPPC/POPG-d_{31} (7:3) which contains fewer deuterated chains. A more significant difference between the spectral series in Fig. 1a and b is the rate at which the fraction of each lipid in the ordered phase grows with decreasing temperature. The higher proportion of gel phase spectral component in DPPC-d_{62}/POPG (7:3) (Fig. 1a), compared with DPPC/POPG-d_{31} (7:3) (Fig. 1b) at corresponding temperatures, in the two phase range, reflects the stronger tendency of POPG to resist ordering.

Figure 1c shows spectra at selected temperatures for DPPC-d_{62}/POPG (7:3) with 3.5% (w/w) SP-$B_{8–25}$ incorporated. The higher resolution of the liquid crystalline spectrum for this sample may reflect a peptide-induced change in the effect of POPG on DPPC-d_{62} dynamics. In addition, the behaviour of this dispersion through the transition region is significantly different from that of the corresponding lipid mixture with no peptide present. As temperature is lowered from 36 to 32°C, doublet splittings increase significantly, indicating increased orientational order, but spectra in this range remain indicative of axially symmetric reorientation. Below 32°C, the spectrum broadens continuously into one characteristic of the gel phase without displaying a superposition of liquid crystal and gel spectral components at any temperature. For DPPC/POPG-d_{31} (7:3) plus 3.5% (w/w) SP-$B_{8–25}$ (Fig. 1d), the increase in splittings of the axially symmetric spectrum before it begins broadening into the gel phase spectrum is not as large but the change from liquid crystal to gel is again continuous with no significant superposition of liquid crystal and gel components.

One interesting consequence of the continuous phase change displayed by both peptide-containing samples (Figs. 1c, d) is that the gel-like spectra at temperatures around 28°C, for which the motion has departed significantly from axially symmetric, still display prominent

shoulders at approximately ±19 kHz. As noted below, the persistence of a spectral feature with this splitting below the transition is reflected in the temperature dependence of the first spectral moments for these samples.

Figure 2 shows the result of applying a de-Pake-ing transform (McCabe and Wassall 1995) to the 38°C spectrum for each sample to obtain spectra corresponding to a single bilayer orientation. Comparison of individual doublet splittings for corresponding samples with and without peptide shows that the peptide increases chain orientational order slightly for both lipids in the liquid crystalline phase.

For a bilayer system containing lipids with perdeuterated saturated chains, the first moment of the ^{2}H-NMR spectrum is proportional to average orientational order of the deuterated chains and is given by

$$M_1 = \frac{\int_0^\infty \omega f(\omega) d\omega}{\int_0^\infty f(\omega) d\omega} \quad (1)$$

where $f(\omega)$ is the spectrum. Figure 3 shows the temperature dependence of M_1 for each of the lipid mixtures with and without SP-B_{8-25} incorporated. Figure 3a shows M_1 for a control sample of DPPC-d_{62}/POPG (7:3) and average values of M_1 for two samples of this lipid mixture containing SP-B_{8-25}. Error bars for the peptide-containing sample points were estimated by calculating the deviation from the mean for pairs of measurements at each temperature and averaging those deviations, separately, for temperatures above and below the transition midpoint. Figure 3b shows

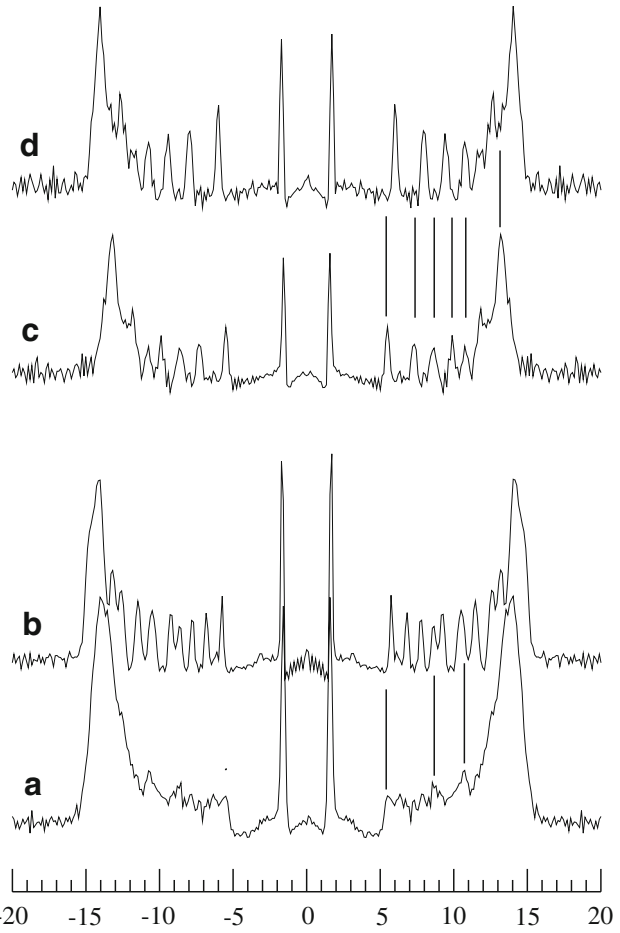

Fig. 2 Spectra corresponding to a single bilayer orientation (normal perpendicular to magnetic field) obtained by applying a de-Pake-ing transform to ^{2}H-NMR spectra for **a** DPPC-d_{62}/POPG (7:3), **b** DPPC-d_{62}/POPG (7:3) + 3.5% N-terminal SP-B peptide, **c** DPPC/POPG-d_{31} (7:3), and **d** DPPC/POPG-d_{31} (7:3) + 3.5% N-terminal SP-B peptide at 38°C. *Vertical lines* are to aid comparison of splittings for corresponding spectra with and without peptide

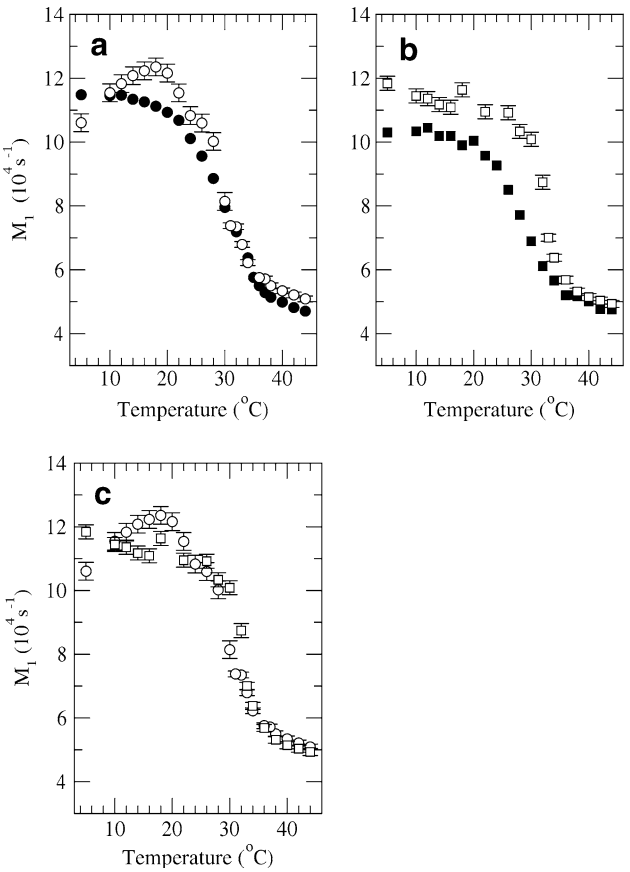

Fig. 3 **a** Temperature dependence of ^{2}H-NMR first spectral moments for DPPC-d_{62}/POPG (7:3) (*solid circle*) and for DPPC-d_{62}/POPG (7:3) + 3.5% N-terminal SP-B peptide (*open circle*). **b** Temperature dependence of ^{2}H-NMR first spectral moments for DPPC/POPG-d_{31} (7:3) (*solid square*) and for DPPC/POPG-d_{31} (7:3) + 3.5% N-terminal SP-B peptide (*open square*). **c** Comparison of first spectral moments for DPPC-d_{62}/POPG (7:3) + 3.5% N-terminal SP-B peptide (*open circle*) and for DPPC/POPG-d_{31} (7:3) + 3.5% N-terminal SP-B peptide (*open square*). *Open symbols* are averages of results for two independent preparations of each peptide-containing sample. *Error bars* were estimated by averaging the deviation from the mean for pairs of measurements at each temperature above and below the transition midpoint. All samples were hydrated in TRIS buffer containing 5 mM Ca^{2+} at pH 7.4

M_1 results for corresponding samples containing DPPC/POPG-d_{31} (7:3).

For both peptide-free samples, M_1 goes from low values, characteristic of liquid crystalline phase, to high values, characteristic of the more ordered gel, as the sample is cooled through the range of temperatures in which spectra are observed to be superpositions of liquid crystal and gel components. Below the transition, M_1 values are higher for DPPC-d_{62}/POPG (7:3) than for DPPC/POPG-d_{31} (7:3). This suggests that in the gel phase, the saturated chains of POPG-d_{31} are more sensitive to local disruption of chain packing by the neighbouring oleyol chain of POPG than are the saturated chains of DPPC-d_{62} in the same mixture.

Figure 3a, b also show M_1 values for the two lipid mixtures with SP-$B_{8–25}$ present. In DPPC-d_{62}/POPG (7:3) (Fig. 3a), the presence of the peptide slightly increases average DPPC-d_{62} chain orientational order in the liquid crystalline phase as noted above with regard to Fig. 2. The temperature range over which M_1 increases at the transition is not significantly changed by the peptide despite the apparent absence of macroscopic phase separation in the presence of the peptide. An inflection, at 31–32°C, in the plot of M_1 vs T for DPPC-d_{62}/POPG plus peptide was apparent in both of the data sets, from independent preparations of that mixture, that were averaged to obtain the open symbols in Fig. 3a. The temperature of this inflection coincides with a rounding of the prominent doublet edges characteristic of axially symmetric reorientation at higher temperature. The apparent peak in the values of M_1 just below the transition temperature range coincides with the persistence of prominent shoulders in the gel-like spectra below 30°C for the DPPC-d_{62}/POPG (7:3) plus SP-$B_{8–25}$ mixture.

In DPPC/POPG-d_{31} (7:3) (Fig. 3b), presence of the peptide again has only a slight ordering effect in the liquid crystal phase. Across the transition range of temperatures, though, M_1 values for the peptide-containing samples are significantly increased relative to the corresponding lipid-only sample. The DPPC/POPG-d_{31} (7:3) bilayers with peptide present also display significantly higher M_1 values, just below the transition temperature range, than the corresponding lipid-only samples but do not give rise to such a prominent peak in M_1 just below the transition.

Figure 3c compares the temperature dependence of M_1 for peptide-containing samples of both lipid mixtures. It is apparent that the M_1 values for the labelled lipids in the DPPC/POPG mixtures are more similar in the presence of SP-$B_{8–25}$ than in the lipid-only bilayers.

Figure 4 shows DSC scans, obtained prior to concentration and addition of calcium, for the two lipid mixtures with and without peptide present. Superimposed traces show the results of consecutive scans on each sample. Taking into account the effects of chain perdeuteration on the transitions temperatures of one or the other lipid component, the scans for DPPC-d_{62}/POPG (7:3) and DPPC/POPG-d_{31} (7:3) are in good agreement with earlier DSC results for non-deuterated mixtures of DPPC and POPG at the same ratio (Wiedmann et al. 1993). In DSC scans of DPPC-d_{62}/POPG (7:3) and DPPC/POPG-d_{31} (7:3) suspensions with calcium added (not shown), the completion temperature of the transition was found to be 1–2°C higher than for the corresponding lipid-only samples without calcium present. Despite the difference in calcium content between the DSC and NMR suspensions, there is satisfactory agreement between the width of the transitions inferred from DSC scans (Figs. 4a–d) and from the temperature dependences of M_1 for corresponding samples (Fig. 3).

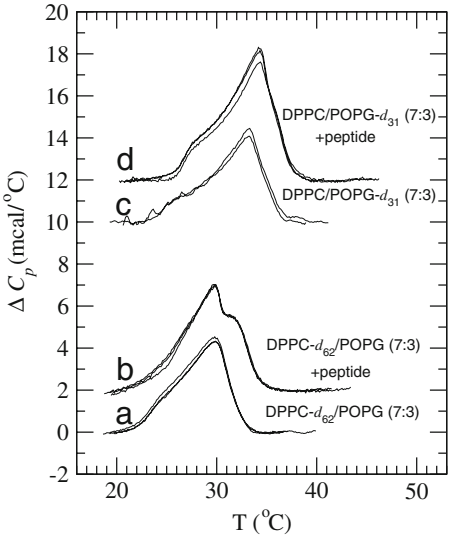

Fig. 4 Differential scanning calorimetry traces for **a** DPPC-d_{62}/POPG (7:3), **b** DPPC-d_{62}/POPG (7:3) + 3.5% N-terminal SP-B peptide, **c** DPPC/POPG-d_{31} (7:3), and **d** DPPC/POPG-d_{31} (7:3) + 3.5% N-terminal SP-B peptide. Samples contained 3 mg of lipid and were suspended in 1.2 ml of TRIS buffer in the absence of Ca^{2+}. *Superimposed traces* show the results of consecutive scans on each sample

Quadrupole echo decay experiments reflect lipid reorientations with correlation times comparable to the $\sim 10^{-5}$ s characteristic time of the ^{2}H-NMR experiment. The decay rate for the echo component corresponding to a particular deuteron is the sum of echo decay rate contributions from each of the motions that modulates the quadrupole interaction experienced by that deuteron. The initial rate at which an observed echo decays with increasing 2τ is a weighted averaged over all of the observed deuterons. The quadrupole echo decay times reported here are the inverse of this averaged echo decay rate.

Figure 5 shows the temperature dependence of quadrupole echo decay times for each of the lipid mixtures with

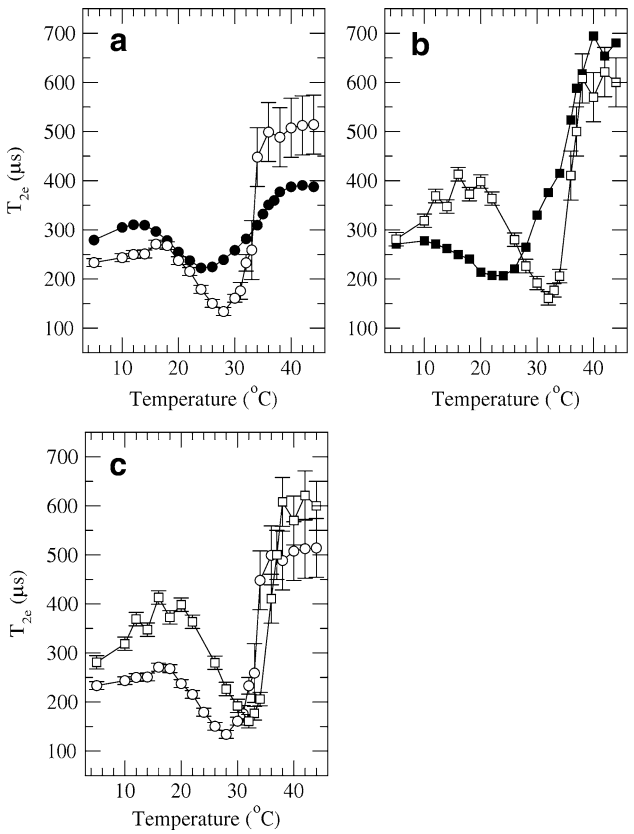

Fig. 5 **a** Temperature dependence of ^{2}H-NMR quadrupole echo decay times for DPPC-d_{62}/POPG (7:3) (*solid circle*) and for DPPC-d_{62}/POPG (7:3) + 3.5% N-terminal SP-B peptide (*open circle*). **b** Temperature dependence of ^{2}H-NMR quadrupole echo decay times for DPPC/POPG-d_{31} (7:3) (*solid square*) and for DPPC/POPG-d_{31} (7:3) + 3.5% N-terminal SP-B peptide (*open square*). **c** Comparison of quadrupole echo decay times for DPPC-d_{62}/POPG (7:3) + 3.5% N-terminal SP-B peptide (*open circle*) and for DPPC/POPG-d_{31} (7:3) + 3.5% N-terminal SP-B peptide (*open square*). *Error bars* were estimated by averaging the deviation from the mean for pairs of measurements at each temperature above and below the transition midpoint. All samples were hydrated in TRIS buffer containing 5 mM Ca^{2+} at pH 7.4

and without SP-$B_{8–25}$ incorporated. In the liquid crystalline phase, there are contributions to the echo decay rate from slow motions, such as bilayer undulations and diffusion over curved bilayer surfaces, and from faster local motions such as fluctuations of overall chain orientation and possibly rotation about the bilayer normal. The contributions to echo decay rate from slower motions decrease as temperature is lowered and correlation times increase (Bloom and Sternin 1987; Weisz et al. 1992). Contributions from these motions can be sensitive to morphology of the multilamellar vesicle samples (Stohrer et al. 1991). Contributions to echo decay rate from faster motions increase along with increasing correlation times as temperature is lowered toward the transition. The weak dependence of echo decay rate on temperature in the liquid crystalline phase, as seen in Fig. 5a for DPPC-d_{62}/POPG (7:3) without peptide, may be a net effect of contributions from both fast and slow motions. As temperature is lowered through the range of two phase coexistence, contributions to echo decay rate from undulations and diffusion continue to decrease but more local single-molecule motions slow and begin to contribute strongly to echo decay rate below the transition. The result is a minimum in average echo decay time near the midpoint of the transition range. As the temperature is lowered further, contributions to echo decay rate from local rotations decrease as these motions continue to slow further. The maximum in echo decay time near 12–14°C reflects the onset of significant contributions from trans-gauche isomerization to echo decay rate.

The temperature dependence of the average echo decay time for DPPC/POPG-d_{31} (7:3) bilayers in the absence of peptide is shown in Fig. 5b. In the liquid crystalline phase, the average echo decay time is longer for POPG-d_{31} than for DPPC-d_{62} in the corresponding mixture but echo decay in the liquid crystalline phase can be sensitive to details of vesicle morphology and the observed difference may not indicate differences between the local environments of the two lipid components. In the peptide-free mixtures, both lipids do, however, pass through similar echo decay time minima. For temperatures below the minimum, echo decay time increases more slowly with decreasing temperature for POPG- d_{31} than for DPPC-d_{62} in the corresponding mixture. This likely indicates that single-molecule motions freeze out more slowly with decreasing temperature for POPG- d_{31} than for DPPC-d_{62}.

Addition of SP-$B_{8–25}$ affects the two lipid species in the mixed bilayers differently. In the liquid crystalline phase of DPPC-d_{62}/POPG (7:3), addition of SP-$B_{8–25}$ tends to raise the echo decay time and thus decrease average echo decay rate. In the liquid crystalline phase of DPPC/POPG-d_{31} (7:3), the effect of SP-$B_{8–25}$, if anything, is to lower the average echo decay time which would correspond to an increase in average echo decay rate. Through the transition and below, the contributions to echo decay rate from slower motions like bilayer undulations, which might be sensitive to vesicle morphology, become less significant and echo decay times are more reproducible. Below the transition midpoint, echo decay is presumably dominated by single-molecule reorientations moving into the slow motion regime for these temperatures. For both lipids in the mixture, the presence of SP-$B_{8–25}$ results in a deeper echo decay time minimum near the transition midpoint and a more rapid increase in echo decay time below the minimum as motions contributing to echo decay in the gel phase freeze out. For temperatures below the onset of the transition, the peptide-induced change in echo decay behaviour is more substantial for POPG-d_{31} in the DPPC/

POPG-d_{31} (7:3) than for DPPC-d_{62} in the corresponding mixture.

Figure 5c compares the temperature behaviours of the quadrupole echo decay times for DPPC-d_{62}/POPG (7:3) plus 3.5 % SP-$B_{8–25}$ and DPPC/POPG-d_{31} (7:3) plus 3.5% SP-$B_{8–25}$. Addition of the peptide results in the quadrupole echo time behaviours of the two lipid components being slightly more similar to each other than in the peptide-free mixtures above the transition midpoint and slightly less similar to each other than in the peptide-free mixtures below the transition midpoint.

Discussion

^{2}H NMR was recently used to compare the perturbing effects of full-length SP-B on DPPC-d_{62} and DPPG-d_{62} in DPPC/DPPG (7:3) mixed bilayers with one or the other lipid component labelled (Morrow et al. 2007). The mixing properties of components in DPPC/DPPG bilayers are dominated by interactions in the headgroup region of the bilayer. The temperatures for which two phase coexistence was observed were above the main transition temperature for DPPC-d_{62} alone ($\sim$37°C) which likely reflects interaction of Ca^{2+} with DPPG. Average chain orientational order was similar for both lipid components in peptide-free DPPC/DPPG bilayer mixtures. Addition of 13% SP-B (w/w) reduced chain order of both lipid components, both above and below the transition. SP-B had little effect on the temperature range over which two phase coexistence was apparent in the DPPC-d_{62}/DPPG (7:3) bilayers and even narrowed that temperature range slightly in the DPPC/DPPG-d_{62} (7:3) bilayers. The results of the current study, involving a peptide based on the N-terminal helix of SP-B and a DPPC/POPG lipid mixture rather than DPPC/DPPG, differ from the earlier study in interesting ways.

In the present work, two phase coexistence in both the DPPC-d_{62}/POPG and DPPC/POPG-d_{31} mixtures, as seen in Figs. 1a, c, is limited to temperatures below the DPPC-d_{62} transition temperature and extends over a range of at least 10 degrees. In contrast, phase separation in DPPC/DPPG (7:3) mixtures, which did not approximate the proportions of saturated and unsaturated chains in natural surfactant, was limited to a narrower range of temperatures (Morrow et al. 2007).

The observation of distinct liquid crystal and gel spectral components implies that coexisting domains must be large enough that lipid environments are not averaged by diffusion across domain boundaries in the characteristic timescale ($\sim 10^{-5}$ s) of the ^{2}H-NMR experiment. Using a lateral diffusion constant of $\sim 1 \times 10^{-11}$ m^2/s for fluid DPPC bilayers (Karakatsanis and Bayerl 1996), rms displacement during the ^{2}H-NMR characteristic time is $\sim$20 nm. The observation of distinct liquid crystal and gel spectral components through the transition range of the lipid-only samples thus suggests that coexisting domains must have dimensions larger than this characteristic length.

The M_1 results in Figs. 3a, b show that addition of 3.5% (w/w) SP-$B_{8–25}$ sharpens the transition of the DPPC/POPG-d_{31} mixture slightly but has little effect on the width of the transition in the DPPC-d_{62}/POPG mixture. More significantly, for both peptide-containing mixtures through the transition temperature range, the spectra (Figs. 1c, d) cannot be resolved into distinct liquid crystal and gel spectral components. This places an upper limit of a few tens of nanometers on the dimensions of any coexisting liquid crystal and gel phase domains near the transition of this mixture in the presence of SP-$B_{8–25}$. In effect, the peptide interferes with the tendency of DPPC and POPG components to phase separate near the bilayer transition temperature. This is particularly interesting in light of recent reports of nanometer-scale domains on compression of functional lung surfactant extract monolayers (Zuo et al. 2008b) and the observation that SP-B promotes the formation of nanometer-scale domain networks upon compression of DPPC and DPPC/DPPG monolayers (Cruz et al. 2004). The observation that this positively charged peptide tends to promote more homogeneous mixing of zwitterionic and anionic lipid components in this model system also suggests that electrostatic interactions alone may not be sufficient to account for the effect of SP-$B_{8–25}$ on DPPC/POPG mixing.

As can be seen from M_1 results in Figs. 2, 3, addition of SP-$B_{8–25}$ raises average chain orientational order slightly for both lipids in the liquid crystalline phase and more substantially in the gel phase. This is qualitatively different from the effect of full-length SP-B on DPPC/DPPG (7:3) for which SP-B was found to reduce orientational order of both lipid components both above and below the transition temperature range. This difference may reflect the difference in unsaturated chain content between the lipid mixtures used in the two studies as well as differences in the effects of full-length SP-B and the SP-$B_{8–25}$ peptide.

In general, whether accommodation of an additional component in a bilayer raises or lowers average chain orientational order is correlated with whether that component promotes, respectively, a decrease or an increase in average headgroup area per lipid relative to average chain area per lipid. If an amphipathic peptide is located closer to the headgroup level in a bilayer, it might be expected to increase the average separation of lipid headgroups and contribute to an average decrease in lipid chain orientational order. If the amphipathic peptide can locate deeper in the membrane, the resulting reduction in lateral space available to chains may be greater than the corresponding reduction in space available to the headgroups resulting in

a peptide-induced increase in lipid chain order. The positively charged residues on SP-B are arginine and lysine. In both of these amino acid types, the positive charge is located at the end of a flexible sidechain so that accommodation of the positive charges in the bilayer headgroup region does not preclude a much deeper location for the bulk of the peptide helix. The difference between the effects of SP-B and SP-$B_{8–25}$ on the chain orders of DPPC/DPPG and DPPC/POPG respectively might thus reflect a deeper average location, in the corresponding bilayer, for SP-$B_{8–25}$ than for full-length SP-B. It should be noted, though, that for a given average saturated chain orientational order, the corresponding available average area per lipid headgroup should be greater in DPPC/POPG bilayers than in DPPC/DPPG bilayers due to the average effect of the oleoyl chain on area per lipid. This would be expected to increase the susceptibility of the DPPC/POPG bilayer to chain ordering influences and may also contribute to the observed differences between responses of the two lipid systems to either full-length SP-B or SP-$B_{8–25}$ peptide.

The NMR spectra of DPPC-d_{62}/POPG (7:3) and DPPC/POPG-d_{31} (7:3) (Fig. 1) are indicative of significant phase separation and two-phase coexistence through the transition. Spectra for the corresponding samples containing SP-$B_{8–25}$ change more continuously through the transition which indicates a more homogeneous mixing of the lipid components on the NMR time scale. Despite this significant difference, the DSC observations do not indicate a substantial change in width or enthalpy of the mixture transition in the presence of SP-$B_{8–25}$. Assuming lipid masses of 3 mg for each of the DSC samples, the observed transition peak areas in Fig. 4 correspond to average lipid transition enthalpies of 6.9 kcal/mole and 7.0 kcal/mole for DPPC-d_{62}/POPG (7:3) and DPPC/POPG-d_{31} (7:3) respectively and 8.2 kcal/mole and 9.1 kcal/mole for the corresponding mixtures containing SP-$B_{8–25}$. Given the width of these transitions, however, baselines can only be approximately determined and the difference between these transition enthalpies may not be significant. It is interesting to note, though, that the change in M_1, and thus average chain orientational order, through the transition (Fig. 3) is slightly larger for the samples containing peptide than for the corresponding lipid-only samples. It is also interesting to note that a weighted average (7:3) of the reported transition enthalpies for DPPC (Mabrey and Sturtevant 1976) and POPG (Fleming and Keough 1983) is ~7.9 kcal/mole. The similarity of this value to the transition enthalpies observed here is consistent with the limited effect that peptide is observed to have on lipid chain packing both above or below the transition. The NMR and DSC observations both show that, regardless of its effect on observable phase separation, the peptide has little effect on the overall width of the transition.

Perturbation of the transition temperature of one or the other lipid component, by deuteration, is not expected to qualitatively change the phase behaviour of the mixture but the shape of the excess heat capacity trace can be affected. In particular, the prominence of a plateau on the high temperature edge of the peak for DPPC-d_{62}/POPG plus peptide (Fig. 4b), compared with magnitude of this feature in the corresponding trace for DPPC/POPG-d_{31} plus peptide (Fig. 4d), likely results from the shift in peak heat capacity resulting from deuteration of the higher- versus the lower-melting lipid component. It is significant that the difference between the shapes of the DSC traces for the peptide-containing samples are consistent with difference between the corresponding first-moment plots. For DPPC-d_{62}/POPG plus peptide, the plateau on the high temperature edge of the excess heat capacity peak seems to correspond with the inflection observed in M_1 versus T (Fig. 3a). For DPPC/POPG-d_{31} plus peptide, the slight shift of the excess heat capacity peak toward the higher temperature edge of the transition corresponds to the sharper increase M_1 as temperature of this sample is lowered through the transition (Fig. 3b).

In a quadrupole echo experiment, the amplitude, $A(2\tau)$ of the echo at time 2τ following the initial pulse is a sum of contributions from deuteron populations experiencing different motions so that

$$A(2\tau) = \sum_i A_i e^{-2\tau R_i} \tag{2}$$

where A_i is proportional to the number of deuterons in a given population and R_i is the sum of contributions to the quadrupole echo decay rate from the set of motions modulating the quadrupole interaction for that population of deuterons. For short times, the observed echo decay time is the inverse of the weighted average of the echo decay rates for all deuterons in the sample.

The extent to which the quadrupole interaction of a specified deuteron is modulated by a given motion, j, can be characterised by the second moment, ΔM_2^j, of that modulation. Motions can be classified as fast if $\tau_j \ll \Delta M_2^j$ or slow if $\tau_j \gg \Delta M_2^j$ (Bloom and Sternin 1987). For fast motions, $R_j = \Delta M_2^j \tau_j$, whereas for slow motions, $R_j \propto \tau_j^{-1}$ (Bloom and Sternin 1987; Pauls et al. 1985). Because correlation times generally increase with decreasing temperature, contributions to echo decay rate tend to increase with decreasing temperature for fast motions and decrease with decreasing temperature for slow motions. The result is a maximum in the contribution to echo decay rate as a given motion passes from fast to slow upon cooling of a bilayer sample.

Despite efforts to minimise differences in average vesicle morphologies by carefully controlling hydration protocols, the possibility of significantly different contributions from

slow motions to echo decay in the liquid crystalline phases of DPPC-d_{62}/POPG (7:3) and DPPC/POPG-d_{31} (7:3) (solid symbols in Figs. 5a, b respectively) cannot be ruled out. It is thus difficult to draw conclusions from the observed difference between the decay times of the two lipids in the liquid crystalline phase of this mixture. As temperature is lowered through the transition region, echo decay times for both lipids in the peptide-free mixture pass through similar minima. For temperatures below the minimum, echo decay time increases more slowly with decreasing temperature for POPG-d_{31} than for DPPC-d_{62} in the corresponding mixture. This implies that single-molecule reorientations, which increasingly dominate quadrupole echo decay as the sample is cooled into the gel phase, freeze out more slowly with decreasing temperature for POPG- d_{31} than for DPPC-d_{62} in corresponding bilayers. This may reflect a local disordering effect of the unsaturated oleoyl chain on POPG.

In the presence of peptide, the quadrupole echo decay times for the two lipid components in the liquid crystalline phase become more similar. While interpretation of quadrupole echo decay in the liquid crystalline phase is complicated by the sensitivity of slow motion contributions to details of vesicle morphology that can be difficult to control, it is clear that interaction with the peptide does not significantly increase differences in the motions of the two lipids in the liquid crystalline phase.

Below the echo decay time minimum, echo decay times for both lipid components in the peptide-containing samples increase more quickly with decreasing temperature than for the same lipids in the peptide-free samples. In effect, addition of SP-$B_{8–25}$ deepens and sharpens the echo decay time minimum. This implies that the correlation times for motions that dominate echo decay, over this temperature range, increase more quickly with decreasing temperature in the presence of the peptide than in the peptide-free bilayers. The peptide-induced change in echo decay time behaviour over this temperature range is larger for the POPG-d_{31} component than for the DPPC-d_{62} component in these mixtures suggesting that the peptide counters the tendency of the POPG to resist freezing out of local rotational motions as temperature is lowered below the transition midpoint.

Because echo decay below the transition midpoint is dominated by more local motions which have slowed into the slow motion regime, interpretation of differences near and below the transition is simpler than in the liquid crystalline phase. In the absence of peptide, single-molecule POPG-d_{31} motions freeze out more slowly with decreasing temperature, below the transition, than the corresponding DPPC-d_{62} motions. Addition of the peptide increases the correlation times, at a given temperature, for local motions of both lipids but the resulting change is larger for POPG-d_{31} than for DPPC-d_{62}, suggesting that addition of peptide reduces difference between the local environments of the two lipid components at temperatures below the transition midpoint.

The observed effects of the SP-$B_{8–25}$ peptide on quadrupole echo decay times for the two lipid components are thus consistent with the suggestion, from inspection of the spectra, that SP-$B_{8–25}$ interferes with the tendency of the saturated-chain DPPC and the mixed-chain POPG to phase separate. This is most apparent through the transition where, in the absence of peptide, it is possible to spectroscopically distinguish domains enriched in DPPC from domains enriched in POPG. The echo decay results suggest that even below the transition, where the samples are spectroscopically homogeneous, the peptide alters the local environments of DPPC and POPG, possibly by decreasing the tendency of the two components to self-aggregate.

The possibility that at least a portion of SP-B promotes more thorough mixing of saturated PC and unsaturated PG lipid components, in mixtures approximating the unsaturated chain content of natural surfactant, may have interesting implications for the behaviour of lung surfactant material particularly under conditions of lateral compression which might be expected to enhance the propensity for saturated and unsaturated lipid components to segregate. Comparing the effects, on model surfactant mixtures, of SP-$B_{8–25}$ with those of other SP-B-derived peptides and full-length SP-B should provide insight into the ways in which the different SP-B helices, and interactions between those helices, contribute to the role of SP-B in functional surfactant.

Acknowledgments This research was supported by a Natural Sciences and Engineering Research Council Undergraduate Student Research Award to B. R.-S. and by grants from the Natural Science and Engineering Research Council of Canada to M. R. M. and from the Canadian Institutes of Health Research to V. B.

References

Andersson M, Curstedt T, Jornvall H, Johansson J (1995) An amphipathic helical motif common to tumourolytic polypeptide NK-lysin and pulmonary surfactant polypeptide SP-B. FEBS Lett 362:328–332. doi:10.1016/0014-5793(95)00268-E

Antharam VC, Farver RS, Kuznetsova A, Sippel KH, Mills FD, Elliott DW, Sternin E, Long JR (2008) Interactions of the C-terminus of lung surfactant protein B with lipid bilayers are modulated by acyl chain saturation. Biochim Biophys Acta 1778:2544–2554. doi:10.1016/j.bbamem.2008.07.013

Bartlett GR (1959) Phosphorus assay in column chromatography. J Biol Chem 234:466–468

Beck DC, Ikegami M, Na CL, Zaltash S, Johansson J, Whitsett JA, Weaver TE (2000) The role of homodimers in surfactant protein B function in vivo. J Biol Chem 275:3365–3370. doi:10.1074/jbc.275.5.3365

Bloom M, Sternin E (1987) Transverse nuclear spin relaxation in phospholipids bilayer membranes. Biochemistry 26:2101–2105. doi:10.1021/bi00382a007

Booth V, Waring AJ, Walther FJ, Keough KMW (2004) NMR structures of the C-terminal segment of surfactant protein B I detergent micelles and hexafluoro-2-propanaol. Biochemistry 43:15187–15194. doi:10.1021/bi0481895

Clark JC, Wert SE, Bachurski CJ, Stahlman MT, Stripp BR, Weaver TE, Whitsett JA (1995) Targetted disruption of the surfactant protein B gene disrupts surfactant homeostasis, causing respiratory failure in newborn mice. Proc Natl Acad Sci USA 92:7794–7798. doi:10.1073/pnas.92.17.7794

Clements JA (1957) Surface tension of lung extracts. Proc Soc Exp Biol Med 95:170–172

Cruz A, Vázquez L, Vélez M, Pérez-Gil J (2004) Effect of pulmonary surfactant protein SP-B on the micro- and nanostructure of phospholipids films. Biophys J 86:308–320. doi:10.1016/S0006-3495(04)74106-5

Davis JH (1979) Deuterium magnetic resonance study of the gel and liquid crystalline phases of dipalmitoyl phosphatidylcholine. Biophys J 27:339–358. doi:10.1016/S0006-3495(79)85222-4

Davis JH, Jeffrey KR, Bloom M, Valic MI, Higgs TP (1976) Quadrupole echo deuteron magnetic resonance spectroscopy in ordered hydrocarbon chains. Chem Phys Lett 42:390–394. doi:10.1016/0009-2614(76)80392-2

Dico AS, Hancock J, Morrow MR, Stewart J, Harris S, Keough KMW (1997) Pulmonary surfactant protein SP-B interacts similarly with dipalmitoylphosphatidylglycerol and dipalmitoylphosphatidylcholine in phosphatidylcholine/phosphatidylglycerol mixtures. Biochemistry 36:4172–4177. doi:10.1021/bi962693v

Fleming BD, Keough KMW (1983) Thermotropic mesomorphism in aqueous dispersions of 1-palmitoyl-2-oleoyl- and 1, 2-dilauroyl-phosphatidylglycerols in the presence of excess Na^{+} or Ca^{2+}. Can J Biochem Cell Biol 61:882–891

Goerke J (1998) Pulmonary surfactant: functions and molecular composition. Biochim Biophys Acta 1408:79–89

Hawgood S, Derrick M, Poulain F (1998) Structure and properties of surfactant protein B. Biochim Biophys Acta 1408:150–160

Johansson J, Curstedt T, Jornvall H (1991) Surfactant protein B: disulfide bridges, structural properties, and kringle similarities. Biochemistry 30:6917–6921. doi:10.1021/bi00242a015

Karakatsanis P, Bayerl TM (1996) Diffusion measurements in oriented phospholipids bilayers by ^{1}H-NMR in a static fringe field gradient. Phys Rev E Stat Phys Plasmas Fluids Relat Interdiscip Topics 54:1785–1790. doi:10.1103/PhysRevE.54.1785

Keough KMW (1998) Lung surfactant: cellular and molecular processing. In: Rooney SA (ed) Surfactant composition and extracellular transformations. R. G. Landes, Georgetown, pp 1–27

Keough KMW, Kariel N (1987) Differential scanning calorimetric studies of aqueous dispersions of phosphatidylcholines containing two polyenoic chains. Biochim Biophys Acta 902:11–18. doi:10.1016/0005-2736(87)90130-1

Kurutz JW, Lee KY (2002) NMR structure of lung surfactant peptide SP-B(11–25). Biochemistry 41:9627–9636. doi:10.1021/bi016077x

Mabrey S, Sturtevant JM (1976) Investigation of phase transitions of lipids and lipid mixtures by high sensitivity differential scanning calorimetry. Proc Natl Acad Sci USA 73:3862–3866. doi:10.1073/pnas.73.11.3862

Manzanares D, Rodriguez-Capote K, Liu S, Haines T, Ramos Y, Zhao L, Doherty-Kirby A, Lajoie G, Possmayer F (2007) Modification of tryptophan and methionine residues is implicated in the oxidative inactivation of surfactant protein B. Biochemistry 46:5604–5615. doi:10.1021/bi062304p

McCabe MA, Wassall SR (1995) Fast-Fourier transform dePaking. J Magn Reson Ser B 106:80–82. doi:10.1006/jmrb.1995.1013

Morrow MR, Pèrez-Gil J, Simatos G, Boland C, Stewart J, Absolom D, Sarin V, Keough KMW (1993) Pulmonary surfactant-associated protein SP-B has little effect on acyl chains in dipalmitoylphosphatidylcholine dispersions. Biochemistry 32:4397–4402. doi:10.1021/bi00067a032

Morrow MR, Stewart J, Taneva S, Dico A, Keough KMW (2004) Perturbation of DPPC bilayers by high concentrations of pulmonary surfactant protein SP-B. Eur Biophys J 33:285–290. doi:10.1007/s00249-003-0357-0

Morrow MR, Temple S, Stewart J, Keough KMW (2007) Comparison of DPPC and DPPG environments in pulmonary surfactant models. Biophys J 93:164–175. doi:10.1529/biophysj.106.102681

Nogee LM, Garnier G, Dietz HC, Singer L, Murphy AM, deMello DE, Colten HR (1994) A mutation in the surfactant protein B gene responsible for fatal neonatal respiratory disease in multiple kindreds. J Clin Invest 93:1860–1863. doi:10.1172/JCI117173

Pastrana-Rios B, Flach CR, Brauner JW, Mautone AJ, Mendelsohn R (1994) A direct test of the "squeeze-out" hypothesis of lung surfactant function. External reflection FT-IR at the air/water interface. Biochemistry 33:5121–5127. doi:10.1021/bi00183a016

Pattle RE (1955) Properties, function and origin of the alveolar lining layer. Nature 175:1125–1126. doi:10.1038/1751125b0

Pauls KP, MacKay AL, Söderman O, Bloom M, Tangea AK, Hodges RS (1985) Dynamic properties of the backbone of an integral membrane peptide measured by ^{2}H-NMR. Eur Biophys J 12:1–11. doi:10.1007/BF00254089

Perez-Gil J, Keough KMW (1998) Interfacial properties of surfactant proteins. Biochim Biophys Acta 1408:203–217

Postle AD, Heeley EL, Wilton DC (2001) A comparison of the molecular species compositions of mammalian lung surfactant phospholipids. Comp Biochem Physiol A Mol Integr Physiol 129:65–73. doi:10.1016/S1095-6433(01)00306-3

Prosser RS, Davis JH, Dahlquist FW, Lindorfer MA (1991) ^{2}H nuclear magnetic resonance of the gramicidin A backbone in a phospholipid bilayer. Biochemistry 30:4687–4696. doi:10.1021/bi00233a008

Revak SD, Merritt TA, Degryse E, Stefani L, Courtney M, Hallman M, Cochrane CG (1988) Use of human surfactant low molecular weight apoproteins in the reconstitution of surfactant biologic activity. J Clin Invest 81:826–833. doi:10.1172/JCI113391

Revak SD, Merritt TA, Hallman M, Heldt G, Polla RJL, Hoey K, Houghten RA, Cochrane CG (1991) The use of synthetic peptides in the formation of biophysically and biologically active pulmonary surfactants. Pediatr Res 29:460–465. doi:10.1203/00006450-199105010-00010

Ryan MA, Qi X, Serrano AG, Ikegami M, Pérez-Gil J, Johansson J, Weaver TE (2005) Mapping and analysis of the lytic and fusogenic domains of surfactant protein B. Biochemistry 44:861–872. doi:10.1021/bi0485575

Sarker M, Waring AJ, Walther FJ, Keough KMW, Booth V (2007) Structure of mini-B, a functional fragment of surfactant protein B, in detergent micelles. Biochemistry 46:11047–11056. doi:10.1021/bi7011756

Serrano AG, Ryan M, Weaver TE, Pérez-Gil J (2006) Critical structure-function determinants within the N-terminal region of pulmonary surfactant protein SP-B. Biophys J 90:238–249. doi:10.1529/biophysj.105.073403

Stohrer J, Gröbner G, Reimer D, Weisz K, Mayer C, Kothe G (1991) Collective lipid motions in bilayer membranes studied by transverse deuteron spin relaxation. J Chem Phys 95:672–678

Vandenbussche G, Clercx A, Clercx M, Curstedt T, Johansson J, Jornvall H, Ruysschaert JM (1992) Secondary structure and

orientation of the surfactant protein SP-B in a lipid environment. A Fourier transform infrared spectroscopy study. Biochemistry 31:9169–9176. doi:10.1021/bi00153a008

Veldhuizen R, Nag K, Orgeig S, Possmayer F (1998) The role of lipids in pulmonary surfactant. Biochim Biophys Acta 1408: 90–108

Veldhuizen EJ, Waring AJ, Walther FJ, Batenburg JJ, van Golde LM, Haagsman HP (2000) Dimeric N-terminal segment of human surfactant protein B (dSP-B(1–25)) has enhanced surface properties compared to monomeric SP-B(1–25). Biophys J 79:377–384. doi:10.1016/S0006-3495(00)76299-0

Walther FJ, Hernandez-Juviel JM, Gordon LM, Sherman MA, Waring AJ (2002) Dimeric surfactant protein B peptide SP-B(1–25) in neonatal and acute respiratory distress syndrome. Exp Lung Res 28:623–640. doi:10.1080/01902140260426733

Weisz K, Gröbner G, Mayer C, Stohrer J, Kothe G (1992) Deuteron nuclear magnetic resonance study of the dynamic organization of phospholipids/cholesterol bilayer membranes: molecular properties and viscoelastic behaviour. Biochemistry 31:1100–1112. doi:10.1021/bi00119a019

Wiedmann T, Salmon A, Wong V (1993) Phase behaviour of mixtures of DPPC and POPG. Biochim Biophys Acta 1167: 114–120

Yu SH, Smith N, Harding PGR, Possmayer F (1983) Bovine pulmonary surfactant: chemical composition and physical properties. Lipids 18:522–529. doi:10.1007/BF02535391

Zasadzinski JA, Ding J, Warriner HE, Bringezu F, Waring AJ (2001) The physics and physiology of lung surfactants. Curr Opin Colloid Interface Sci 6:506–511. doi:10.1016/S1359-0294(01)00124-8

Zuo YY, Veldhuizen RAW, Neumann AW, Petersen NO, Possmayer F (2008a) Current perspectives in pulmonary surfactant—inhibition, enhancement, and evaluation. Biochim Biophys Acta 1778:1947–1977. doi:10.1016/j.bbamem.2008.03.021

Zuo YY, Keating E, Zhao L, Tadayyon SM, Veldhuizen RAW, Petersen NO, Possmayer F (2008b) Atomic force microscopy studies of functional and dysfunctional pulmonary surfactant films. I. Micro- and nanostructures of functional pulmonary surfactant films and the effect of SP-A. Biophys J 94:3549–3564. doi:10.1529/biophysj.107.122648